Desalination and Water Treatment
www.deswater.com

doi: 10.1080/19443994.2015.1128985

57 (2016) 21842–21854
October

Taylor & Francis
Taylor & Francis Group

Facile synthesis of β-FeOOH nanoparticle-loaded secondary fly ash composites for enhanced removal of copper ion

Heng Yang[a,b], Qi Zhou[a,b], Wenjun Luo[a], Chunjie Yan[a,b,*]

[a]*Faculty of Material and Chemistry, China University of Geosciences, Wuhan 430074, China, Tel./Fax: +86 27 67885098; emails: yh061053@126.com (H. Yang), roundzking@163.com (Q. Zhou), wandering_in_field@126.com (W. Luo), chjyan2005@126.com (C. Yan)*

[b]*Engineering Research Center of Nano-Geomaterials of Education Ministry, China University of Geosciences, Lu Mo Road 388, Wuhan 430074, China*

Received 1 April 2015; Accepted 30 November 2015

ABSTRACT

Based on the "treating wastewater with wastes" strategy, an acid-dissolved fly ash residue derived from the extracting aluminum industry (denoted as secondary fly ash (SFA)) was chosen as very cheap and suitable solid support to be modified as an adsorbent for the removal of Cu^{2+} from wastewater in this article. A facile liquid-phase deposition method was introduced to achieve the loading of active β-FeOOH nanoparticles on the SFA surface wherein the gelatin was added to regulate microstructure and dispersity of the nanoparticles. The texture and composition of products were characterized using various techniques such as FE-SEM, XRF, X-ray diffraction, N_2 adsorption/desorption, and ^{27}Al MAS NMR. Results of batch adsorption experiments showed that SFA-Fe exhibited an obviously enhanced adsorption performance than the raw one. The optimal adsorption of Cu^{2+} was achieved at pH 5.5, and high temperature was beneficial to the adsorption with an increasing adsorption capacity (12.59−14.91 mg g^{-1}) as environment temperatures rise from 298.15 to 318.15 K. The experimental data were determined to be well described by the pseudo-second-order kinetics and Freundlich isotherm model. Furthermore, thermodynamic analysis revealed that the adsorption process of Cu^{2+} by SFA-Fe is endothermic and spontaneous. In addition, the electrostatic interactions and proton exchange are manifested to be the two main mechanisms for Cu^{2+} adsorption. This investigation not only provides a utilization approach of the SFA but also fabricates a potential and low-cost adsorbent for treatment of Cu^{2+} contamination.

Keywords: Cu^{2+} adsorption; β-FeOOH nanoparticle; Secondary fly ash; Surface modification; Adsorption mechanism

1. Introduction

With the development of the industrialization, heavy metal pollution is grave which has aroused more and more attention in the world. As it is non-biodegradable and has the characteristics of bioaccumulation, hence has toxicity toward lives [1], it would be of great significance to remove it before being discharged into nature water system. Copper ion (Cu^{2+}) is one of the typical heavy metal contaminants in

*Corresponding author.

water which has widespread presence in the industrial applications, e.g. electrical, electro-plating, metal-finishing, and paint industries. Various approaches have been used for Cu^{2+} removal from wastewater, such as chemical precipitation [2], electrochemical treatment [3], membrane filtration [4], solvent extraction [5,6], biosorption [7,8], ion-exchange [9], and adsorption [10]. Nevertheless, most of them have their own disadvantages and limitations, such as secondary pollution, complicated treatment processes, high cost and energy consumption [11–14], leading to marginally cost-effective or difficult to implement especially in developing countries. Among these methods, adsorption operation is regarded as a potential technique for wastewater treatment which can overcome these shortcomings [15–17], wherein development of a cost-effective, high-efficient adsorbent is the key, and corresponding preparation technology is urgently desiderated.

Generally, a material is considered to be of low-cost if it has abundant sources, or is either a by-product or a waste from another industry. Coal fly ash, a well-known solid waste, have a large production throughout the world every year due to the increasing demand for energy leading to an increase in the utilization of coal [18,19]. Despite a considerable portion of fly ash is used in relevant industry, such as construction or soil amendment, there is still a large portion that is directly disposed to the environment [20]. Such disposal is not economic and environmentally sound [21]. Alternative way to utilize fly ash as absorbent in water treatment has brought a lot of interest because of its physical and chemical adsorption properties from oxide composition, surface polarity, size fractions, cost of cheapness, and the advantage based on waste control by waste, meanwhile endue with adjunctive value to this material [22–25].

The Shenhua Group Zhungeer electric power station is one of China's largest electric power plants utilizing coal and subsequently producing a plenty of coal fly ash [26]. Due to the geographical features, these fly ash have the unique characteristic of high alumina content (>50%), which can be regarded as secondary resources for recovery of valuable aluminum from them [27,28]. Thus, extracting alumina industry by an acid leaching process has been developed by Shenhua Group. Due to the dissolution of metal oxides, the structure of fly ash was seriously damaged and the acid-dissolved fly ash particles residue (named as secondary fly ash (SFA)) had a severely corroded surface, fine granularity, and rich porosity, which was found to be a very cheap and suitable solid support to be modified as an adsorbent. Loading metal (hydr)oxide on the carrier surface as active component has been proved to be a feasible modification route to dramatically strengthen the adsorption performance. For instance, it was reported that the deposition of manganese oxide on the surface of alkali-treated diatomite could make it more effective for metal ions removal than original one by a 2.4-fold increase in the adsorbent surface area [29].

In this work, iron (hydr)oxide nanoparticles were chosen to be loaded on the surface of SFA to obtain an effective adsorbent for Cu^{2+} removal from contaminated water owing to its high affinity for metal species [30–34]. The fabrication of the composite was achieved by a facile liquid-phase deposition method: the iron hydroxide colloid was first prepared by a simple forced hydrolysis process as the reaction $Fe^{3+} + 2H_2O \rightarrow FeO(OH) + 3H^+$ under a mild condition, and then the rod-like β-FeOOH nanoparticles were deposited on the SFA substrate at the aging period by introducing gelatin as dispersant for mediating the aggregation of nanoparticles and regulating the growth of the β-FeOOH crystals through the polar group ($–COO^-$ and $–NH_2$) in gelatin linear macromolecule. Such nanoparticle assembly mechanism mediated by this bio-template has also been reported previously in the formation of other metal oxides [35–38]. The objectives of this investigation were (i) to prepare a novel adsorbent of β-FeOOH nanoparticle-loaded SFA by a facile method; (ii) to systematically study the adsorption characteristics and mechanism of SFA-Fe adsorbent for Cu^{2+} in batch experiments as a function of contact time, solution pH, initial concentration, and temperature.

2. Materials and methods

2.1. Chemicals and materials

The SFA used in this study was the industrial residue after extracting alumina process by acid leaching from Shenhua Group Zhungeer Energy Co., Ltd. The main particle size of the SFA was about 2.0–5.0 μm by sieving. All other chemicals were of analytical grade and commercially available from Shanghai Chemical Reagent Co., Ltd and used as received without further purification. Distilled water was used throughout the experiments for solution preparation.

2.2. Synthesis of SFA-Fe

Purifying the SFA involved a heat pretreatment process in a programed temperature controlled muffle oven at 900°C for 4 h.

Iron-modified SFA samples were prepared according to the following procedures: 2.00 g SFA was added in 100 mL of 1.0% gelatin solution and then 1.62 g

(0.01 M) $FeCl_3$ was dissolved into the mixture solution. The mixture was stirred vigorously for 0.5 h to facilitate uniform dispersion of SFA particles followed by being heated to boiling for 10 min, then placed in the oven to be aged for another 24 h at 90℃. The solid product (i.e. SFA-Fe) was filtered, washed repeatedly with deionized water, and dried at 60℃ overnight.

2.3. Characterization of materials

The bulk chemical composition in samples melted with lithium tetraborate was performed with an XRF PANalytical B.V. AxiosMAX spectrometer. X-ray diffraction analysis (XRD) to investigate crystalline structures were carried out on a Germany Bruker D8-FOCUS powder X-ray diffractometer, using CuKα radiation ($\lambda = 0.154$ nm) (40 kV, 30 mA) over the scanning range $2\theta = 10^\circ$–70° with a step width of 2°/min. Surface morphology of the sample surfaces (SEM) analyses were examined on a Hitachi SU8010 field emission scanning electron microscope, operated at 5 kV, in powder samples coated with Au. ^{27}Al MAS NMR spectrum was collected on a Bruker Avance III 500 MHz solid-state NMR spectrometer with pulse width of 0.25 μs, recycle delay time of 1 s, and spinning speed of 12 kHz, using 1.0 M $Al(NO_3)_3$ aqueous solution as the reference solutions. The surface area, pore size, and pore volume of samples were analyzed by N_2adsorption/desorption method using automatic surface area analyzer (ASAP2020, US).

2.4. Adsorption experiments

Batch adsorption experiments were conducted to investigate the property of SFA-Fe for the removal of Cu^{2+} from aqueous solution. The synthetic aqueous solutions of Cu^{2+} were prepared by the dissolution of $Cu(NO_3)\cdot 3H_2O$ in deionized water. Typical adsorption procedure was carried out as follows: 0.01 g adsorbent and 20 mL of 50 mg L^{-1} standard Cu^{2+} solution were mixed into a vial, and then the mixture was shaken with speed of 200 rpm in a shaker at 298.15 K for 36 h (until adsorption equilibrium). Afterward, the suspensions were filtered using a 0.22-μm syringe filter made of polypropylene membrane, and concentrations of Cu^{2+} were determined using the inductive coupled plasma emission spectrometer (ICP) (DGS-III single channel scanning spectrometer instrument, Shanghai Tailun Co., Ltd, China). Adsorption capacity was calculated by the following equation:

$$q_e = (C_0 - C_e)\frac{V}{m} \quad (1)$$

where q_e is the sorption capacity at equilibrium (mg g^{-1}), C_0 is the initial concentration of Cu^{2+} (mg L^{-1}), C_e is the equilibrium concentration of Cu^{2+} (mg L^{-1}), V is the volume of Cu^{2+} solutions, and m is the mass of the adsorbent (g).

The effect of solution pH on adsorption of Cu^{2+} was investigated in the pH range of 2.0−5.5 adjusted with dilute NaOH and HCl through a similar procedure described above. At optimal pH, kinetic experiments were carried out by adsorption for a specified time (1–36 h). To evaluate the adsorption equilibrium and thermodynamic properties, isothermal adsorption experiments were conducted over a range of initial Cu^{2+} concentrations from 5 to 100 mg L^{-1} at three different temperatures of 298.15, 308.15, and 318.15 K, respectively.

3. Results and discussion

3.1. Characterization of materials

The chemical composition of the raw FA, SFA, and the SFA-Fe determined by XRF are listed in Table 1. It can be found that the raw FA has very considerable alumina content which is above 50%. Then, a significant reduction in the alumina content has been observed in SFA after Al-leaching compared with the raw one, but the SFA is still rich in Al_2O_3 (26.25%). To explain this phenomenon, the characterization results of ^{27}Al MAS NMR spectrum for the raw FA and SFA are also provided in Fig. 1, which show that the 4-coordinated Al and 6-coordinated Al are the main existence forms in both of the two samples. According to the quantitative results of ^{27}Al MAS NMR spectrum, the content of 4-coordinated Al are 48.1 and 26.3% for

Table 1
Chemical composition of raw FA, SFA, and SFA-Fe (mass %)

Sample	Raw FA	SFA	SFA-Fe
SiO_2	27.35	65.385	35.144
Al_2O_3	50.85	26.246	14.107
TFe_2O_3	2.01	0.519	40.35
MgO	0.28	0.056	0.03
CaO	5.41	0.552	0.297
Na_2O	0.04	0.091	0.049
K_2O	0.33	0.239	0.128
MnO	–	0.01	0.005
TiO_2	2.12	4.15	2.23
P_2O_5	–	0.099	0.053
Mass loss	7.74	–	6.18
Total	96.13	97.347	98.573

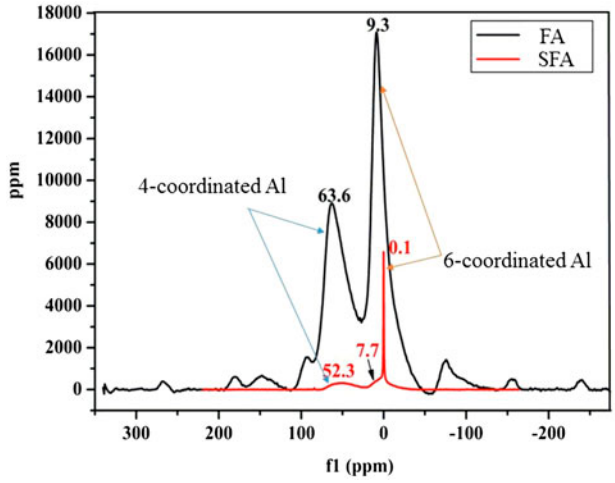

Fig. 1. ^{27}Al MAS NMR spectrum of the raw FA and SFA.

FA and SFA, respectively; this means that in the process of Al-leaching, 6-coordinated Al content increase (73.70%), while 4-coordinated Al content decrease. So we can conclude that the aluminum extracted from fly ash is almost the 4-coordinated Al, and the 6-coordinated Al is much stable in the acid leaching process by with an enormous amount remained in the SFA solid residue.

Moreover, from Table 1, the successful coating of β-FeOOH onto SFA can also be confirmed by the arresting increase in iron content from 0.52 to 40.35% after being modification.

The XRD patterns of adsorbents (SFA and SFA-Fe) are shown in Fig. 2. From Fig. 2(a), the mullite (PDF card no. 02-0431) and anatase (PDF card no. 71-1168) in addition to quartz (PDF card no. 02-0471) can be found in this SFA sample as the main mineral phases. Differing from the original SFA, there are some new diffraction peaks of 11.8˚, 16.8˚, 26.6˚, and 35.2˚ observed in the diffraction pattern of Fig. 2(b), which can be assigned to the (1 1 0), (2 0 0), (3 1 0), and (2 1 1) planes of β-FeOOH crystal, matching well with its standard spinel structure (PDF card no. 34-1266). This observation further suggests that β-FeOOH precipitates were formed on the surface of SFA by the liquid-phase deposition process.

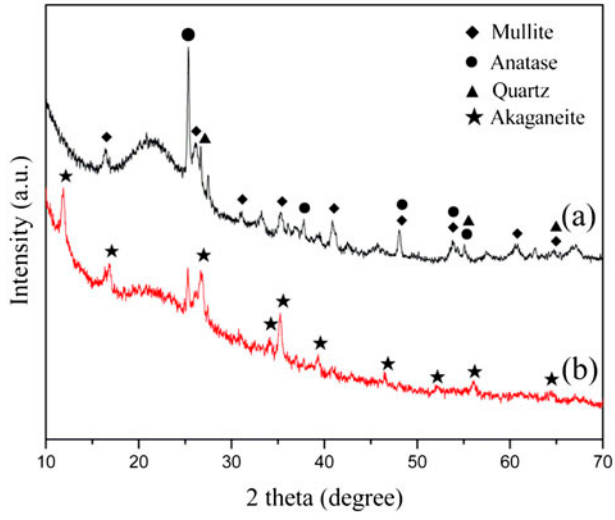

Fig. 2. XRD patterns of (a) SFA and (b) SFA-Fe.

Fig. 3(a) indicates that the original SFA is no rules of granules and lots of pores distributed on its surface and interior. The SEM micrograph of SFA-Fe (Fig. 3(b)) shows that lot of rod-like β-FeOOH nanoparticles have been deposited on the surface of SFA. It should be noted that many pores still can be observed on the substrate, due to that, a certain shape of β-FeOOH particles could not jam in the pores, which should be beneficial for the adsorption. Moreover, the color change of the sample after the preparation process further confirms the successful synthesis of SFA-Fe composite (insets in Fig. 3(a) and (b)).

In addition, for analyzing the pore structure and surface area of the SFA and SFA-Fe, the N_2 adsorption–desorption isotherms as well as pore size distribution curves of these samples are shown in Fig. 4. Both SFA and SFA-Fe show a type II isotherm with a big H3 hysteresis loop in the P/P_0 range of 0.5–1.0, which is usually given by aggregates of adsorbents containing slit-shaped pores. The results of BET surface areas and pore properties are listed in Table 2, which reveal that the modified SFA have much higher parameters compared with the raw SFA. The increase in both pore volume (0.117–0.172 cm^3/g) and pore size (12.46–14.81 nm) should be attributed to the secondary pores resulting from accumulation of rod-like β-FeOOH nanoparticles on the surface of SFA-Fe.

3.2. Mechanisms for Cu^{2+} absorption onto SFA-Fe

Based on the effect of initial pH on adsorption and final pH variation of solution, the mechanisms for the Cu^{2+} removal by the SFA-Fe were analyzed.

3.2.1. Effect of initial pH on adsorption

The solution pH is a very important parameter in the adsorption process. In view of the fact that precipitate CuO are expected to form above pH 5.2, but relatively less between pH 5.2 and 5.5 [39], the initial pH was performed over the range from 2.0 to 5.5. The results of pH effects for SFA and SFA-Fe on Cu^{2+}

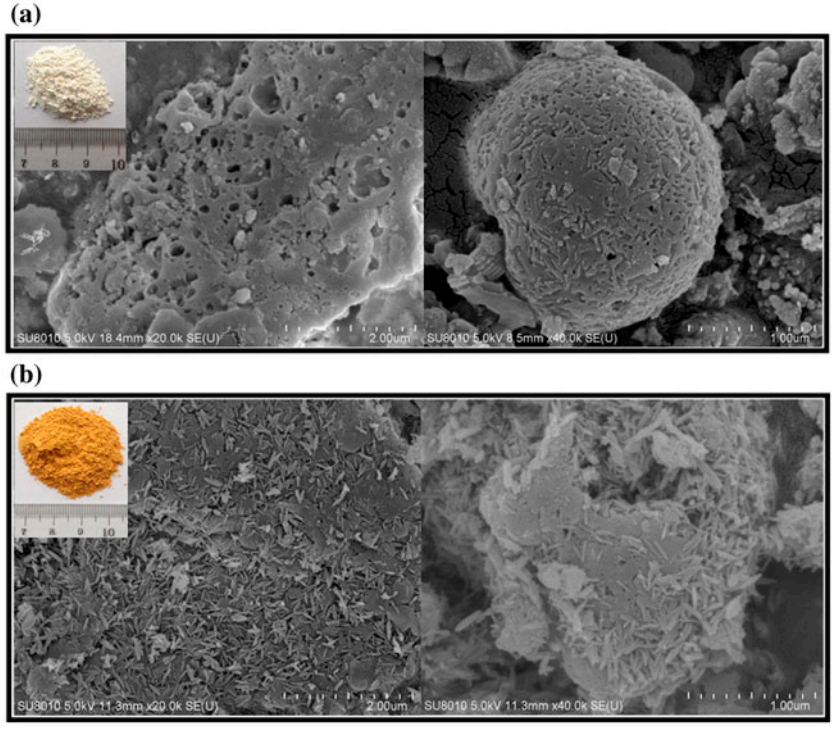

Fig. 3. Typical scanning electron micrographs for (a) SFA and (b) SFA-Fe.

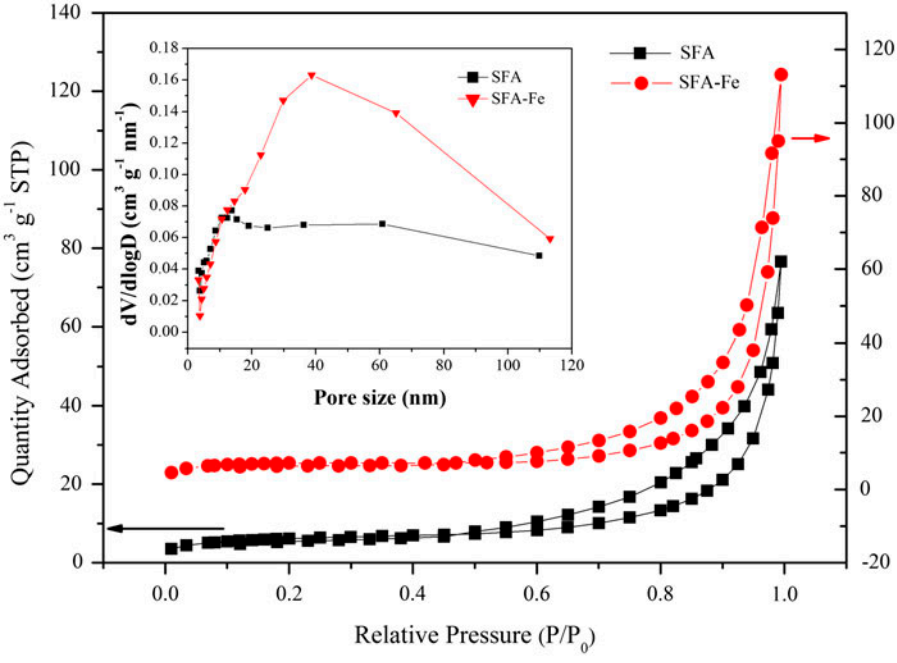

Fig. 4. Nitrogen adsorption–desorption isotherms for SFA and SFA-Fe (Inset shows Barrett–Joyner–Halenda (BJH) pore size distribution).

Table 2
BET surface areas and pore properties of SFA and SFA-Fe

Sample	S_{BET} (m^2/g)	Pore volume (cm^3/g)	Pore size (nm)
SFA	21.9	0.117	12.46
SFA-Fe	24.7	0.172	14.81

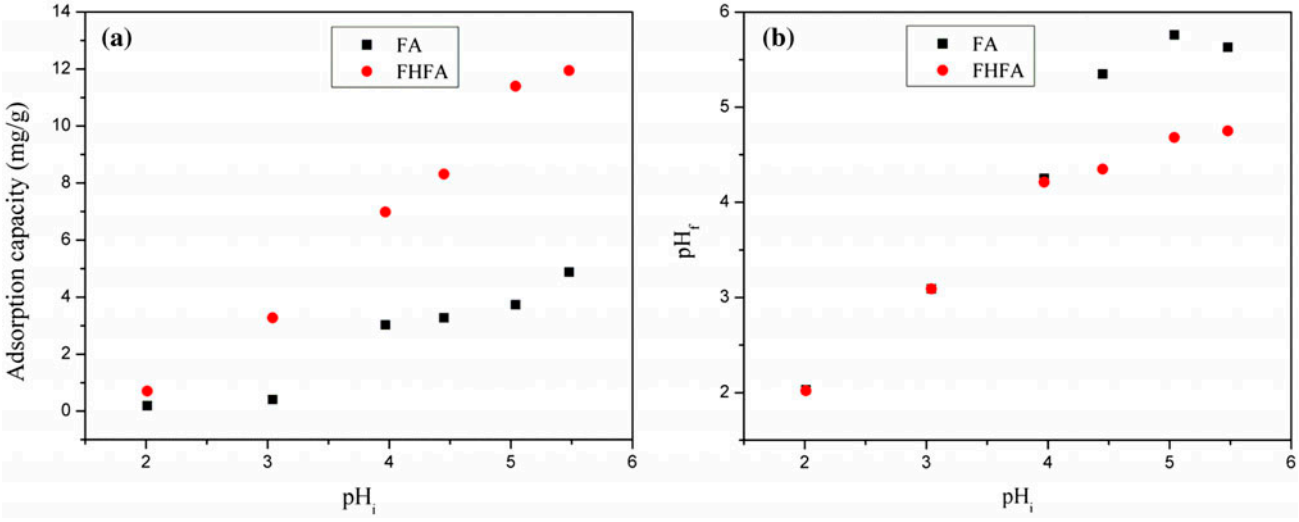

Fig. 5. (a) Effect of initial pH and (b) Change of final pH on the adsorption of Cu^{2+} by SFA and SFA-Fe.

removal are presented in Fig. 5(a). It clearly indicates that the tendency of Cu^{2+} adsorption onto SFA-Fe and SFA are similar, which are both strongly dependent on pH value. The adsorption capacity sharply increases with the pH increases at the value 2.0–4.0 and then rises slowly to reach the maximum at pH 5.5. This adsorption behavior can be explained in terms of the surface charge of the adsorbent depended on the solution pH with the protonation and deprotonation process:

$$XOH + H^+ \leftrightarrow XOH_2^+ \quad \left(pH < pH_{zpc}\right)$$

$$XOH \leftrightarrow XO^- + H^+ \left(pH > pH_{zpc}\right)$$

where X represents the active sites on material surface such as Si, Al, Fe, and XOH represents uncharged surface site, XOH_2^+ represents positively charged surface site, and XO^- represents negative surface site.

The adsorbate in aqueous solution exists mainly as Cu^{2+} in the pH range of 2.0−5.5. Surface hydroxide maybe protonated in acid media, especially when $pH < pH_{zpc}$, the surface of the adsorbent was positively charged, which is unfavorable for the adsorption of Cu^{2+} cation by the electrostatic repulsion. Meanwhile, the low adsorption capacity may also be due to that large number of H^+ in solution compete with Cu^{2+} for the adsorption sites. With the increase in pH, the number of negatively charged hydroxide groups increases, leading to the increased attraction for Cu^{2+}, thus improving the adsorption capacity [40].

Moreover, β-FeOOH deposited on SFA results in higher adsorption capacities for Cu^{2+} than the raw SFA in the whole pH range of 2.0−5.5. Especially, in optimal pH (~5.5), the adsorption capacity of SFA-Fe can be up to be about 2.5 times larger than that of raw SFA, the enhanced adsorption of Cu^{2+} might be attributed to the increasing in specific surface area and pore volume of SFA-Fe.

3.2.2. Final pH variation of solution

Fig. 5(b) shows the change of solution pH after the adsorption process, it is very interesting to observe that the gap, ΔpH, between initial pH and final pH (ΔpH = final pH – initial pH) was diverse. For raw

SFA, the values of ΔpH were positive at the pH range of 2.0−5.5. But the ΔpH of SFA-Fe changed from positive to negative at the point of pH 4.5.

The ΔpH variation can be attributed to the existence of two opposite effects in the adsorption process. On the one hand, the *in situ* formation of surface hydroxyl by attracting the free H^+ or reacting with water on the strong polarity sites of X–O [41] causes a decline trend in H^+ concentration in the solution. On the other hand, the proton exchange occurred between surface hydroxyl and Cu^{2+} in the adsorption process will release H^+ into solution, shown as follows [42]:

$$XOH + Cu^{2+} \leftrightarrow XOCu^{+} + H^{+}$$

$$XOH + Cu^{2+} + H_2O \leftrightarrow XO^{-} \ldots CuOH^{+} + 2H^{+}$$

when the former effect is greater than the latter, the final pH should be higher than the initial pH so that the ΔpH would be positive, the Cu^{2+} adsorbed to raw SFA belonged to this case. But due to more $-OH^-$ sites appearing on the surface of SFA-Fe by the loading of β-FeOOH, the release of H^+ by proton exchange could reduce the final solution pH after the initial pH 4.5.

Through the above analysis, we can confirm that the electrostatic interactions and proton exchange are the two main mechanisms for Cu^{2+} adsorption onto SFA-Fe, The schematic description of the mechanisms is illustrated in Fig. 6.

3.3. Kinetic studies

The adsorption of Cu^{2+} onto SFA-Fe at the concentration of 50 mg L^{-1} determined as a function of contact time is shown in Fig. 7(a). As seen from Fig. 7(a), the adsorption capacities for Cu^{2+} rise steeply with the increase in contact time from the beginning to 18 h. Thereafter, the adsorption uptake continues to increase at a slower rate until approaches equilibrium after 30 h. The result indicates that the adsorption sites on the exterior surface of SFA-Fe is abundant and highly accessible, but with its rapid consumption, the Cu^{2+} ions then diffused into the pores of the adsorbent and were adsorbed on the interior surface of the adsorbent, which should take a relatively long time. In order to elucidate the adsorption kinetic process, the data of Fig. 7(a) were then represented by the nonlinear form of pseudo-first-order (Eq. (2)) and second-order models (Eq. (3)) [43]:

$$q_t = q_e(1 - e^{-k_1 t}) \tag{2}$$

$$q_t = \frac{k_2 q_e^2 t}{(1 + k_2 q_e t)} \tag{3}$$

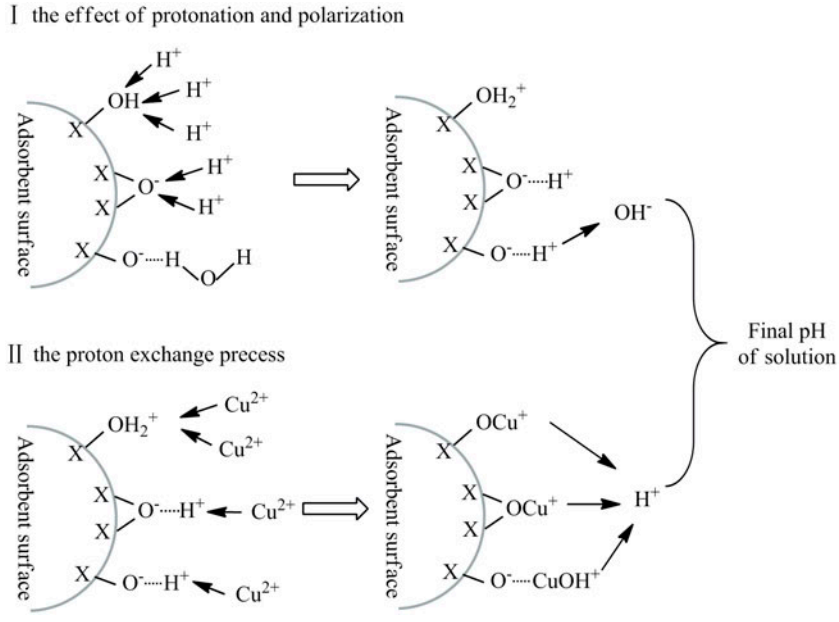

Fig. 6. Sketch illustrating mechanism of Cu^{2+} uptake on adsorbent.

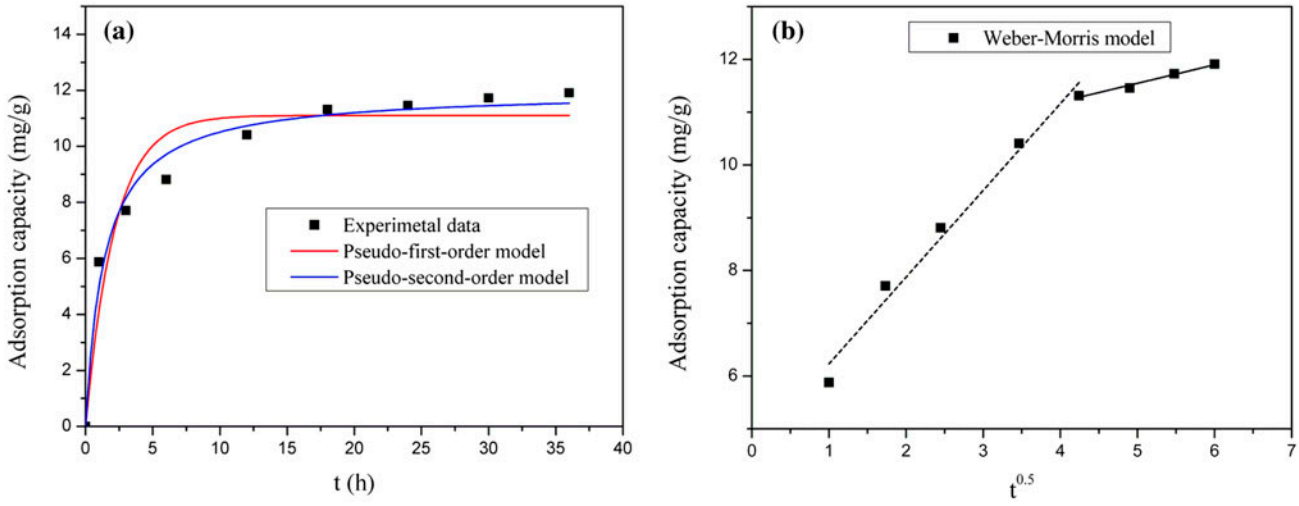

Fig. 7. (a) Nonlinear fitting of pseudo-first-order and pseudo-second-order models and (b) plots of Weber–Morris diffusion model for the adsorption of Cu^{2+} onto SFA-Fe.

Table 3
Coefficients of pseudo-first-order and pseudo-second-order adsorption kinetic models

	Pseudo-first-order model			Pseudo-second-order model		
$q_{e,exp}$ (mg g^{-1})	k_1 (min^{-1})	$q_{e,cal}$ (mg g^{-1})	R^2	k_2 (g mg^{-1} min^{-1})	$q_{e,cal}$ (mg g^{-1})	R^2
11.91	0.465	11.10	0.9366	0.059	11.98	0.9820

where q_t (mg g^{-1}) is the Cu^{2+} sorption capacity at time t, and k_1 (min^{-1}) and k_2 (g mg^{-1} min^{-1}) are the rate constant of pseudo-first-order adsorption and the equilibrium rate constant of pseudo-second-order adsorption, respectively.

The parameters in the kinetic models and the correlation coefficients (R^2) are obtained and given in Table 3. It can be seen that the experimental q_e value is very close to the calculated q_e value for pseudo-second-order kinetic model. Moreover, the R^2 value of the pseudo-second-order model is higher than that of the pseudo-first-order. This confirms that the kinetics of Cu^{2+} adsorption follow the pseudo-second-order model well. This also means that the adsorption rate is proportional to the square of the number of free sites, which corresponds to the term $(q_e - q_t)^2$ in the pseudo-second-order model [44].

Generally, the overall solute adsorption onto the solid surface may be controlled by one or more steps. In order to determine the actual rate-controlling step involved in the Cu^{2+} adsorption process, the well-known Weber–Morris intraparticle diffusion model was applied:

$$q_t = k_i t^{0.5} + C \quad (4)$$

where k_i (g mg^{-1} $min^{-0.5}$) is the intraparticle diffusion rate coefficient, and C (mg g^{-1}) gives an information about the thickness of the boundary layer. These values were determined by a plot of q_t vs. $t^{0.5}$.

As seen from Fig. 7(b), the adsorption data are well fitted by two straight lines and the straight lines deviate from the origin, indicating that two steps took place during Cu^{2+} adsorption onto SFA-Fe [45]: The first linear portion should be attributed to that Cu^{2+} in aqueous solution transported onto the external surface of adsorbent particle (external diffusion) at the early stage of the adsorption. Subsequently, the second linear portion corresponds to the diffusion of Cu^{2+} into the internal sites of adsorbent (intraparticle diffusion or inner diffusion).

The slope and intercept values of two straight lines, along with R^2 values, are listed in Table 4. The R^2 values are close to unity, confirming the applicability of this model. The slope of the linear portion indicates the rate of the adsorption. The lower slope corresponds to a slower adsorption process. This implies that the external diffusion resistance is significant only in the early stage of adsorption and the intraparticle diffusion of Cu^{2+} into pores is the

Table 4
Kinetic parameters calculated from Weber–Morris Model for Cu^{2+} adsorption onto SFA-Fe

	First stage			Second stage		
C_0 (mg L^{-1})	C_1 (mg g^{-1})	$k_{i,1}$ (mg g^{-1} $min^{-0.5}$)	R^2	C_2 (mg g^{-1})	$k_{i,2}$ (mg g^{-1} $min^{-0.5}$)	R^2
50	4.59	1.64	0.977	9.79	0.35	0.970

Table 5
Maximum adsorption capacities for the adsorption of Cu^{2+} onto various adsorbents

Adsorbent	Adsorption capacity (mg g^{-1})	Refs.
Iron oxide-coated sand	2.17	[46]
Iron oxide	17.08	[47]
Wheat shell	8.3	[48]
Eggshell	5.03	[49]
SFA-Fe	11.98[a]	This work

[a]Calculated by pseudo-second-order model.

rate-limiting step in the adsorption process on SFA-Fe, particularly over long contact time periods.

A comparative study of our prepared SFA-Fe to other reported adsorbents is preformed [46–49], and the results are presented in Table 5, which suggests that the SFA-Fe has a fine affinity toward Cu^{2+} ions.

3.4. Equilibrium studies

Fig. 8(a) depicts the adsorption isotherms of Cu^{2+} adsorption by SFA-Fe at various temperatures. Adsorption capacity of SFA-Fe increases with the increase in initial Cu^{2+} concentrations and gradually reaches equilibrium; this may be due to the fact that the adsorbent has surplus adsorption sites for Cu^{2+} at relatively low initial Cu^{2+} concentration but would be saturated at higher concentration. It can also be observed that higher temperature is beneficial to the adsorption with the adsorption capacity from 12.59 to 14.91 mg g^{-1} as temperature is raised from 298.15 to 318.15 K. Generally, the adsorption of adsorbate from the solution phase onto the solid–liquid interface occurs by expelling the solvent molecules (i.e. H_2O) from the interfacial region. With a rise in temperature, the interaction between solvent and solid surface reduced to expose a greater number of adsorption sites, which enhanced the possibility of interaction between the Cu^{2+} and the adsorbent [50].

Analysis of equilibrium data is important for evaluating adsorption properties of SFA-Fe. The widely used Langmuir and Freundlich equations (Eqs. 5 and 6) were applied to describe the adsorption isotherm data by linear forms [51]:

$$\frac{C_e}{q_e} = \frac{1}{Q_0 K_L} + \left(\frac{1}{Q_0}\right) C_e \tag{5}$$

$$\log q_e = \log K_F + \frac{1}{n} \log C_e \tag{6}$$

where C_e is the equilibrium concentration of Cu^{2+} (mg L^{-1}), q_e is the amount of Cu^{2+} adsorbed at equilibrium (mg g^{-1}), Q_0 is the maximum adsorption capacity (mg g^{-1}), and K_L (L g^{-1}) is the Langmuir binding constant, which is related to the energy of adsorption; K_F and n are Freundlich constants representing adsorption capacity and adsorption intensity, respectively.

The fitting curves of Langmuir and Freundlich model are shown in Fig. 8(b) and (c). The estimated adsorption constants with correlation coefficient obtained from the isotherms are listed in Table 6. In terms of the correlation coefficients R^2 values, the experimental data can be well fitted to the Freundlich isotherm model rather than the Langmuir isotherm model, indicating that the adsorption process occurred on a heterogeneous surface and was not restricted to the formation of a monolayer [52]. Moreover, the Freundlich exponent n has a value changing from 1.42 to 2.22, which lies in the range of 1–10 for classification as favorable adsorption, indicating that Cu^{2+} is favorably adsorbed onto SFA-Fe [53].

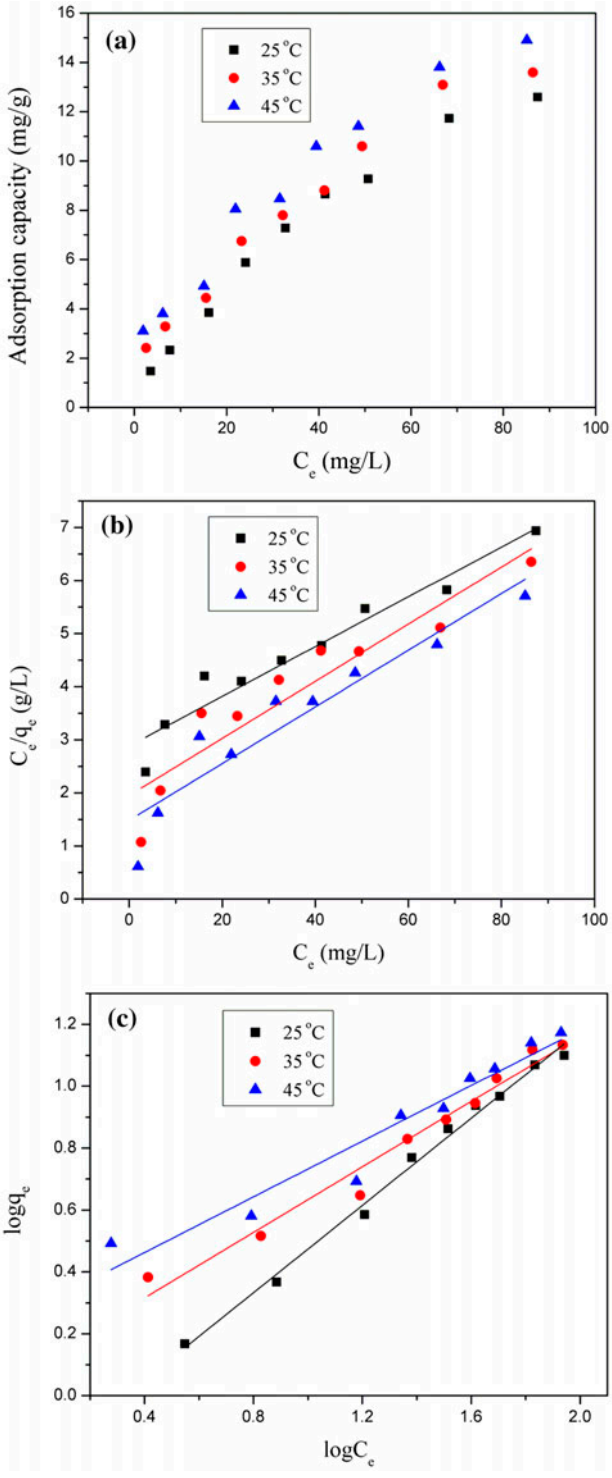

Fig. 8. (a) Isotherms of Cu^{2+} adsorption onto SFA-Fe at different temperatures, (b) linear Langmuir isotherm model, and (c) linear Freundlich isotherm model.

3.5. Thermodynamic studies

Thermodynamic considerations of an adsorption process can give very valuable insight into the nature of the adsorption process. The thermodynamic parameters of free energy of adsorption (ΔG°), enthalpy (ΔH°), and entropy (ΔS°) changes are properly evaluated, which were calculated by the following equations (Eqs. (7) and (8)):

$$\Delta G^\circ = -RT \ln K_c \tag{7}$$

$$\ln K_c = \frac{\Delta S^\circ}{R} \frac{\Delta H^\circ}{RT} \tag{8}$$

where R is universal gas constant (8.314 J mol^{-1} K^{-1}), T is the absolute temperature (K), and K_c is the thermodynamic equilibrium constant which is defined as Eq. (9) [54]:

$$K_c = \frac{\alpha_s}{\alpha_e} = \frac{\gamma_s C_s}{\gamma_e C_e} \tag{9}$$

where α_s is the activity of the adsorbed Cu^{2+}, α_e is the activity of Cu^{2+} in equilibrium solution, C_s is the amount of Cu^{2+} adsorbed by per mass of SFA-Fe (mmol g^{-1}), C_e is the Cu^{2+} concentration in solution at equilibrium (mmol ml^{-1}), γ_s is the activity coefficient of the adsorbed Cu^{2+}, and γ_e is the activity coefficient of Cu^{2+} in equilibrium solution. As the concentration of Cu^{2+} in the solution approaches zero, the activity coefficients (γ_s and γ_e) approach unity, Eq. (10) can be written as:

$$\lim_{C_e \to 0} \frac{\gamma_s C_s}{\gamma_e C_e} = \frac{C_s}{C_e} = K_c \tag{10}$$

values of K_c can be obtained by plotting $\ln(C_s/C_e)$ vs. C_e based on a least-squares analysis and extrapolating C_e to zero [55]. The straight line obtained is fitted to the points based on a least-squares analysis. Its intercept with the vertical axis gives the values of K_c.

The intercept slope of the plot of $\ln K_c$ vs. $1{,}000/T$ is given in Fig. 9, and the obtained thermodynamic parameters are listed in Table 7. The negative values of ΔG° confirm the feasibility of the process and spontaneous adsorption of Cu^{2+} onto SFA-Fe. Moreover, the decrease in negative value of ΔG° (−4.42 kJ mol^{-1} to −4.84 kJ mol^{-1}) with the increase in temperature

Table 6
Adsorption isotherm constants for Cu^{2+} adsorption onto SFA-Fe

	Langmuir isotherm constants			Freundlich isotherm constants		
T (K)	q_m (mg g^{-1})	K_L (L mg^{-1})	R^2	K_F ($mg^{1-1/n}$ $L^{1/n}$ g^{-1})	n	R^2
298.15	21.37	0.016	0.9326	0.59	1.42	0.9922
308.15	18.62	0.028	0.8670	1.27	1.89	0.9696
318.15	18.76	0.036	0.8781	1.92	2.22	0.9310

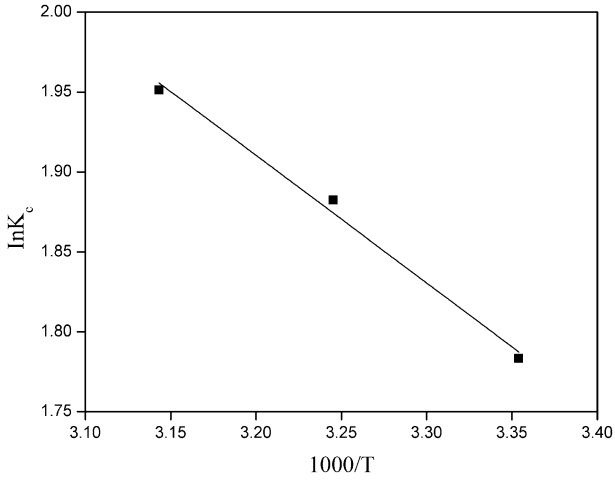

Fig. 9. Plot of ln K_c vs. 1,000/T for estimation of thermodynamic parameter.

Table 7
Thermodynamic parameters for the adsorption of Cu^{2+} onto SFA-Fe

T (K)	298.15	308.15	318.15
K_c	5.95	6.57	7.04
ΔG° (kJ mol^{-1})	−4.42	−4.67	−4.84
ΔS° (J mol^{-1} K^{-1})	37.11		
ΔH° (kJ mol^{-1})	6.63		

indicates that the adsorption process becomes more favorable at higher temperatures. This is possibly because the increase of temperature was beneficial for the mass transfer and adsorption of Cu^{2+} onto adsorbent by expelling the solvent molecules (i.e. H_2O) from the interfacial region. A positive value of ΔH° (6.63 kJ mol^{-1}) indicates that the adsorption process was endothermic in nature. Two main types of adsorption may occur: physical and chemical. The enthalpy change for physical adsorption is usually no more than 4.2 kJ mol^{-1} since the forces are weak; chemical adsorption involves forces much stronger than in physical adsorption, and the enthalpy change for chemical adsorption is more than 21 kJ mol^{-1}, so it seems that both physical and chemical processes were existed in adsorption of Cu^{2+} onto SFA-Fe, but it was more inclined to be a physical process [56]. The positive values of entropy change (ΔS°) show the increased randomness of the solution interface during the adsorption of Cu^{2+} on the adsorbent [57]. Also, the positive ΔS° may be a manifestation of electrostatic interaction between adsorbent and adsorbate [58].

4. Conclusion

In this work, a novel adsorbent of β-FeOOH nanoparticle-loaded SFA composite has been successfully prepared, the iron nanoparticles on the surface of SFA-Fe adsorbent showed good dispersity and regularity. Compared with the raw SFA, the modified SFA exhibited a remarkably enhanced adsorption capacity for the removal of Cu^{2+} with the increase in specific surface area and pore volume. The electrostatic interaction and proton exchange were revealed to be the main adsorption mechanisms. The adsorption property of SFA-Fe for Cu^{2+} was evaluated in detail through a combination of kinetics, equilibriums, and thermodynamics investigation. Results showed that the maximum adsorption capacity could be up to 14.91 mg g^{-1} at 318.15 K under pH 5.5. The adsorption process could be better described by the pseudo-second-order kinetics model, and the adsorption rate was found to be controlled by external diffusion at the initial stage followed by the inner diffusion during the subsequent period. Freundlich model fitted well the isotherms data than Langmuir model, indicating the heterogeneous distribution of active sites on SFA-Fe surface. Furthermore, thermodynamic data suggested that Cu^{2+} adsorption on SFA-Fe was a spontaneous, endothermic, and entropy-driven process. These results suggest that this new composite is qualified for wastewater treatment in the removal of Cu^{2+} as a low cost-effective adsorbent.

Acknowledgments

The authors are grateful for the joint support by the Public Service Project of the Chinese Ministry of Land and Resources (No. 201311024), the Comprehensive Utilization Demonstration Base of Ganzhou Rare Earth Resource sponsored by Chinese Ministry of Land and Resources, the Comprehensive Utilization Research of Refractory Manganese Carbonate Ore in Fenghuang-Huayuan of China and Selenium Resources in Ziyang- Enshi of China (No. 12120113087100).

References

[1] C.O. Adewunmi, W. Becker, O. Kuehnast, F. Oluwole, G. Dörfler, Accumulation of copper, lead and cadmium in freshwater snails in southwestern Nigeria, Sci. Total Environ. 193 (1996) 69–73.
[2] M.M. Matlock, B.S. Howerton, D.A. Atwood, Chemical precipitation of heavy metals from acid mine drainage, Water Res. 36 (2002) 4757–4764.
[3] H. Cheng, Cu(II) Removal from lithium bromide refrigerant by chemical precipitation and electrocoagulation, Sep. Purif. Technol. 52 (2006) 191–195.
[4] H. Bessbousse, T. Rhlalou, J.F. Verchère, L. Lebrun, Removal of heavy metal ions from aqueous solutions by filtration with a novel complexing membrane containing poly(ethyleneimine) in a poly(vinyl alcohol) matrix, J. Membr. Sci. 307 (2008) 249–259.
[5] S. Agarwal, A.E. Ferreira, S. Santos, M.T.A. Reis, M.R.C. Ismael, M. Correia, J.M.R. Carvalho, Separation and recovery of copper from zinc leach liquor by solvent extraction using Acorga M5640, Int. J. Miner. Process. 97 (2010) 85–91.
[6] W. Fu, Q. Chen, H. Hu, C. Niu, Q. Zhu, Solvent extraction of copper from ammoniacal chloride solutions by sterically hindered β-diketone extractants, Sep. Purif. Technol. 80 (2011) 52–58.
[7] L.C. Ajjabi, L. Chouba, Biosorption of Cu^{2+} and Zn^{2+} from aqueous solutions by dried marine green *macroalga Chaetomorpha linum*, J. Environ. Manage. 90 (2009) 3485–3489.
[8] M. Jian, C. Tang, M. Liu, Adsorptive removal of Cu^{2+} from aqueous solution using aerobic granular sludge, Desalin. Water. Treat. 54 (2015) 2005–2014.
[9] H. Shin, J. Song, E. Shin, C. Kang, Ion-exchange adsorption of copper(II) ions on functionalized single-wall carbon nanotubes immobilized on a glassy carbon electrode, Electrochim. Acta 56 (2011) 1082–1088.
[10] S. Rosenzweig, G.A. Sorial, E. Sahle-Demessie, D.C. McAvoy, A.A. Hassan, Effect of chloride ions and water chemistry on copper (II) adsorption on functionalized and pristine carbon nanotubes compared to activated carbon F-400, Water Air Soil Pollut. 225 (2014) 1–17.
[11] F. Fu, Q. Wang, Removal of heavy metal ions from wastewaters: A review, J. Environ. Manage. 92 (2011) 407–418.
[12] H. Chen, G. Dai, J. Zhao, A. Zhong, J. Wu, H. Yan, Removal of copper(II) ions by a biosorbent—*Cinnamomum camphora* leaves powder, J. Hazard. Mater. 177 (2010) 228–236.
[13] N. Das, Recovery of precious metals through biosorption—A review, Hydrometallurgy 103 (2010) 180–189.
[14] S. Sen Gupta, K.G. Bhattacharyya, Kinetics of adsorption of metal ions on inorganic materials: A review, Adv. Colloid Interface Sci. 162 (2011) 39–58.
[15] M. Lehmann, A.I. Zouboulis, K.A. Matis, Removal of metal ions from dilute aqueous solutions: A comparative study of inorganic sorbent materials, Chemosphere 39 (1999) 881–892.
[16] D. Ghosh, K.G. Bhattacharyya, Adsorption of methylene blue on kaolinite, Appl. Clay Sci. 20 (2002) 295–300.
[17] M.J. Santos Yabe, E. de Oliveira, Heavy metals removal in industrial effluents by sequential adsorbent treatment, Adv. Environ. Res. 7 (2003) 263–272.
[18] K.S. Hui, C.Y.H. Chao, Effects of step-change of synthesis temperature on synthesis of zeolite 4A from coal fly ash, Microporous Mesoporous Mater. 88 (2006) 145–151.
[19] J. Yan, D.W. Kirk, C.Q. Jia, X. Liu, Sorption of aqueous phosphorus onto bituminous and lignitous coal ashes, J. Hazard. Mater. 148 (2007) 395–401.
[20] D.G. Grubb, M.a.S. Guimaraes, R. Valencia, Phosphate immobilization using an acidic type F fly ash, J. Hazard. Mater. 76 (2000) 217–236.
[21] R.S. Iyer, J.A. Scott, Power station fly ash—A review of value-added utilization outside of the construction industry, Resour. Conserv. Recycl. 31 (2001) 217–228.
[22] O. Khelifi, Y. Kozuki, H. Murakami, K. Kurata, M. Nishioka, Nutrients adsorption from seawater by new porous carrier made from zeolitized fly ash and slag, Mar. Pollut. Bull. 45 (2002) 311–315.
[23] M. Nascimento, P.S.M. Soares, V.P.d. Souza, V.P.d. Souza, Adsorption of heavy metal cations using coal fly ash modified by hydrothermal method, Fuel 88 (2009) 1714–1719.
[24] C.D. Woolard, J. Strong, C.R. Erasmus, Evaluation of the use of modified coal ash as a potential sorbent for organic waste streams, Appl. Geochem. 17 (2002) 1159–1164.
[25] P. Pengthamkeerati, T. Satapanajaru, P. Chularuengoaksorn, Chemical modification of coal fly ash for the removal of phosphate from aqueous solution, Fuel 87 (2008) 2469–2476.
[26] Z. Zhiming, S. Cotterill, China's first AC powered walking dragline in coal mining, MINExpo. Int'l. (2008). Available from: <https://mining.cat.com/cda/files/2793951/7/scotterill%20paper%20minexpo%20final.pdf>.
[27] M. Lin, G. Bai, P. Duan, J. Xü, D. Duan, Z. Li, Perspective of comprehensive exploitation of the valuable elements of Chinese coal, Energy, Explor. Exploit. 31 (2013) 623–628.
[28] S. Dai, L. Zhao, S. Peng, C.-L. Chou, X. Wang, Y. Zhang, D. Li, Y. Sun, Abundances and distribution of minerals and elements in high-alumina coal fly ash from the Jungar Power Plant, Inner Mongolia, China, Int. J. Coal Geol. 81 (2010) 320–332.
[29] M.A.M. Khraisheh, Y.S. Aldegs, W.A.M. Mcminn, Remediation of wastewater containing heavy metals using raw and modified diatomite, Chem. Eng. J. 99 (2004) 177–184.

[30] M. Villalobos, M.A. Trotz, J.O. Leckie, Surface complexation modeling of carbonate effects on the adsorption of Cr(VI), Pb(II), and U (VI) on goethite, Environ. Sci. Technol. 35 (2001) 3849–3856.
[31] M. Lehmann, A.I. Zouboulis, K.A. Matis, Modelling the sorption of metals from aqueous solutions on goethite fixed-beds, Environ. Pollut. 113 (2001) 121–128.
[32] E.A. Deliyanni, E.N. Peleka, K.A. Matis, Modeling the sorption of metal ions from aqueous solution by iron-based adsorbents, J. Hazard. Mater. 172 (2009) 550–558.
[33] Y.-H. Chen, F.-A. Li, Kinetic study on removal of copper(II) using goethite and hematite nano-photocatalysts, J. Colloid Interface Sci. 347 (2010) 277–281.
[34] C.L. Peacock, D.M. Sherman, Copper(II) sorption onto goethite, hematite and lepidocrocite: A surface complexation model based on ab initio molecular geometries and EXAFS spectroscopy, Geochim. Cosmochim. Acta 68 (2004) 2623–2637.
[35] K.-M. Fang, Z.-Z. Wang, M. Zhang, A.-J. Wang, Z.-Y. Meng, J.-J. Feng, Gelatin-assisted hydrothermal synthesis of single crystalline zinc oxide nanostars and their photocatalytic properties, J. Colloid Interface Sci. 402 (2013) 68–74.
[36] T. Gordon, B. Perlstein, O. Houbara, I. Felner, E. Banin, S. Margel, Synthesis and characterization of zinc/iron oxide composite nanoparticles and their antibacterial properties, Colloids Surf., A: Physicochem. Eng. Aspects 374 (2011) 1–8.
[37] A.F. Costa, P.M. Pimentel, F.M. Aquino, D.M.A. Melo, M.A.F. Melo, I.M.G. Santos, Gelatin synthesis of $CuFe_2O_4$ and $CuFeCrO_4$ ceramic pigments, Mater. Lett. 112 (2013) 58–61.
[38] S.-Z. Kang, T. Wu, X. Li, J. Mu, A facile gelatin-assisted preparation and photocatalytic activity of zinc oxide nanosheets, Colloids Surf., A: Physicochem. Eng. Aspects 369 (2010) 268–271.
[39] J. Guzman, I. Saucedo, J. Revilla, R. Navarro, E. Guibal, Copper sorption by chitosan in the presence of citrate ions: Influence of metal speciation on sorption mechanism and uptake capacities, Int. J. Biol. Macromol. 33 (2003) 57–65.
[40] V.K. Gupta, Equilibrium uptake, sorption dynamics, process development, and column operations for the removal of copper and nickel from aqueous solution and wastewater using activated slag, a low-cost adsorbent, Ind. Eng. Chem. Res. 37 (1998) 192–202.
[41] T. Morimoto, M. Nagao, F. Tokuda, Relation between the amounts of chemisorbed and physisorbed water on metal oxides, J. Phys. Chem. 73 (1969) 243–248.
[42] P.R. Grossl, D.L. Sparks, C.C. Ainsworth, Rapid kinetics of Cu (II) adsorption/desorption on goethite, Environ. Sci. Technol. 28 (1994) 1422–1429.
[43] A.K. Mishra, T. Arockiadoss, S. Ramaprabhu, Study of removal of azo dye by functionalized multi walled carbon nanotubes, Chem. Eng. J. 162 (2010) 1026–1034.
[44] S.A. Ntim, S. Mitra, Removal of trace arsenic to meet drinking water standards using iron oxide coated multiwall carbon nanotubes, J. Chem. Eng. Data 56 (2011) 2077–2083.
[45] Y.S. Ho, G. McKay, Sorption of dye from aqueous solution by peat, Chem. Eng. J. 70 (1998) 115–124.
[46] N. Boujelben, J. Bouzid, Z. Elouear, Adsorption of nickel and copper onto natural iron oxide-coated sand from aqueous solutions: Study in single and binary systems, J. Hazard. Mater. 163 (2009) 376–382.
[47] Y.-H. Huang, C.-L. Hsueh, H.-P. Cheng, L.-C. Su, C.-Y. Chen, Thermodynamics and kinetics of adsorption of Cu(II) onto waste iron oxide, J. Hazard. Mater. 144 (2007) 406–411.
[48] N. Basci, E. Kocadagistan, B. Kocadagistan, Biosorption of copper (II) from aqueous solutions by wheat shell, Desalination 164 (2004) 135–140.
[49] K. Vijayaraghavan, J. Jegan, K. Palanivelu, M. Velan, Removal and recovery of copper from aqueous solution by eggshell in a packed column, Miner. Eng. 18 (2005) 545–547.
[50] M. Ghaedi, A. Hassanzadeh, S.N. Kokhdan, Multiwalled carbon nanotubes as adsorbents for the kinetic and equilibrium study of the removal of alizarin red S and morin, J. Chem. Eng. Data 56 (2011) 2511–2520 .
[51] F. Xie, X. Lin, X. Wu, Z. Xie, Solid phase extraction of lead (II), copper (II), cadmium (II) and nickel (II) using gallic acid-modified silica gel prior to determination by flame atomic absorption spectrometry, Talanta 74 (2008) 836–843.
[52] E. Bulut, M. Özacar, İ.A. Şengil, Equilibrium and kinetic data and process design for adsorption of Congo Red onto bentonite, J. Hazard. Mater. 154 (2008) 613–622.
[53] H.Y. Zhu, Y.Q. Fu, R. Jiang, J.H. Jiang, L. Xiao, G.M. Zeng, S.L. Zhao, Y. Wang, Adsorption removal of congo red onto magnetic cellulose/Fe_3O_4/activated carbon composite: Equilibrium, kinetic and thermodynamic studies, Chem. Eng. J. 173 (2011) 494–502.
[54] S. Wang, Y.-Y. Zhu, S. Wu, W.-J. Luo, H. Xia, C.-G. Zhou, Highly efficient removal of acid red 18 from aqueous solution by magnetically retrievable chitosan/carbon nanotube: Batch study, isotherms, kinetics, and thermodynamics, Chem. Eng. J. 218 (2013) 39–45.
[55] A.A. Khan, R.P. Singh, Adsorption thermodynamics of carbofuran on Sn (IV) arsenosilicate in H^+, Na^+ and Ca^{2+} forms, Colloids Surf. 24 (1987) 33–42.
[56] H.B. Senturk, D. Ozdes, C. Duran, Biosorption of Rhodamine 6G from aqueous solutions onto almond shell (*Prunus dulcis*) as a low cost biosorbent, Desalination 252 (2010) 81–87.
[57] D. Zhao, X. Yang, H. Zhang, C. Chen, X. Wang, Effect of environmental conditions on Pb(II) adsorption on β-MnO_2, Chem. Eng. J. 164 (2010) 49–55.
[58] H. Bian, M. Li, Q. Yu, Z. Chen, J. Tian, H. Liang, Study of the interaction of artemisinin with bovine serum albumin, Int. J. Biol. Macromol. 39 (2006) 291–297.